Journal of Power Sources 189 (2009) 841–846

Contents lists available at ScienceDirect

Journal of Power Sources

journal homepage: www.elsevier.com/locate/jpowsour

Modeling for the scale-up of a lithium-ion polymer battery

Ui Seong Kim [a], Chee Burm Shin [a,*], Chi-Su Kim [b]

[a] Dept. of Chemical Engineering and Division of Energy Systems Research, Ajou University, Suwon 443-749, Republic of Korea
[b] EIG Ltd., R&D Center, Cheonan 330-814, Republic of Korea

ARTICLE INFO

Article history:
Received 28 June 2008
Received in revised form 28 August 2008
Accepted 2 October 2008
Available online 17 October 2008

Keywords:
Lithium-ion polymer battery
Model
Scale-up
Finite element method

ABSTRACT

This paper reports a modeling approach for the scale-up of a lithium-ion polymer battery (LIPB). A comparison of the experimental discharge curves with the modeling results confirmed that the parameters used to model a small-scale LIPB could be applied to a large-scale LIPB provided the materials and composition of the electrodes as well as the processes for manufacturing the batteries were the same. The potential and current-density distribution on the electrodes of a LIPB were predicted as a function of the discharge time using the finite element method. In addition, the temperature distributions of the LIPB were calculated based on the modeling results of the potential and current-density distributions. The temperature distributions from the model were in good agreement with the experimental measurements.

1. Introduction

The lithium-ion polymer battery (LIPB) is a preferred power source for the hybrid electric vehicle (HEV) and electric vehicle (EV) on account of its high energy density, high voltage, low self-discharge rate, and good stability. However, much larger lithium-ion polymer batteries than those currently available in the market for consumer electronics are needed for HEV and EV applications. The performance of a battery electrode is influenced by the aspect ratio of electrodes and the size and placement of the current collecting tabs. If an electrode is not designed optimally, the potential and current density will be distributed non-uniformly, resulting in the non-uniform utilization of the active material over the electrode. Excessive localized utilization of the active material on the electrode will induce an inhomogeneous temperature distribution in the battery during high power extraction, which might cause battery degradation and thermal runaway. This effect becomes more pronounced as the size of the electrode increases. Therefore, optimizing the design of the electrode is essential for the production of large-scale LIPB.

Mathematical modeling can play an important role when scaling up a small-scale battery to a large-scale one because almost limitless design iterations can be performed using simulations [1]. Previous reviews of the modeling of lithium batteries are given in Refs. [2–5]. A one-dimensional model assumes that the gradients of the variables adopted in the model are negligible in the two directions parallel to the current collectors [6–9]. Such an assumption might be valid for small-scale cells but may not be justified for large-scale batteries. This is because the potential drop along the current collector due to ohmic drop may be significant enough to affect the current distribution, with a higher current closer to the tabs. Therefore, a two- or three-dimensional model may be more desirable for large-scale batteries [10–16].

In this study, two-dimensional modeling was performed to calculate the potential and current-density distribution on the electrodes of a LIPB using the same procedure reported by Kwon et al. [17]. They adopted a relatively simple modeling approach by considering only Ohm's law and charge conservation on the electrodes based on the simplified polarization characteristics of the electrodes compared with the papers previously published by other researchers [18–26]. Thermal modeling of the LIPB was carried out based on the modeling results of the potential and current-density distributions using the same procedure described by Kim et al. [27]. The coupling between the models is one-way in the sense that the thermal model depends on the model of potential and current-density distribution, but not vice versa. The modeling presented in this work was applied to the scale-up of a LIPB from 10 to 26 Ah.

2. Mathematical model

A LIPB consisting of a $Li[NiCoMn]O_2$ positive electrode, a graphite negative electrode and a plasticized electrolyte from VK Corporation was modeled in this study. A cell consisting of two parallel plate electrodes of the battery shown in Fig. 1 was chosen

* Corresponding author. Tel.: +82 31 219 2388; fax: +82 31 219 1612.
E-mail address: cbshin@ajou.ac.kr (C.B. Shin).

0378-7753/$ – see front matter © 2008 Elsevier B.V. All rights reserved.
doi:10.1016/j.jpowsour.2008.10.019

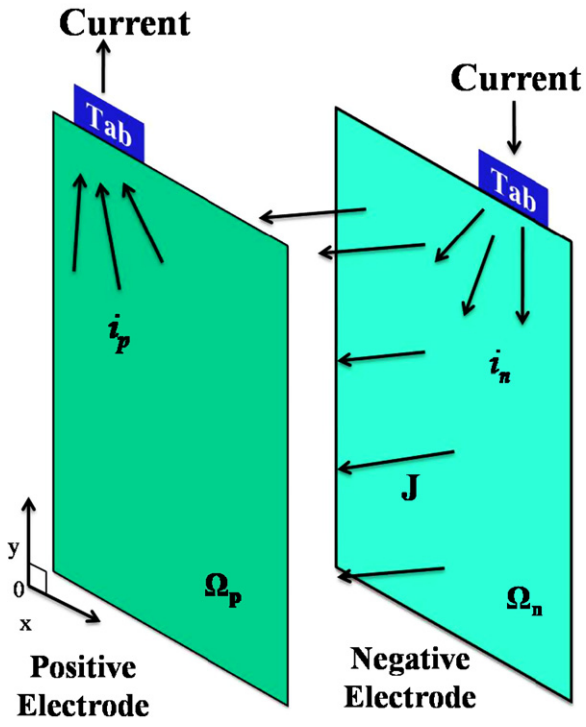

Fig. 1. Schematic diagram of the current flow in the parallel plate electrodes of a battery.

because the battery consists of the same repeating units of positive and negative electrode plates, polymer electrolytes and separators. In Fig. 1, the current collecting tabs are the current collectors extending outside from the rectangular electrodes and they do not contain the electrode (active) material. Fig. 1 shows a schematic diagram of the current flow in the cell during discharge. The distance between the electrodes was assumed to be so small that the current flow between the electrodes would be perpendicular to the electrodes. The modeling procedure used to calculate the potential and current-density distribution on the electrodes was the same as that used by Kwon et al. [17]. From the continuity of current on the electrodes, the following equations can be derived:

$$\nabla \cdot \vec{i}_p - J = 0 \quad \text{in } \Omega_p \tag{1}$$

$$\nabla \cdot \vec{i}_n + J = 0 \quad \text{in } \Omega_n \tag{2}$$

where $\vec{i}_p$ and $\vec{i}_n$ are the linear current-density vectors (current per unit length ($A\,m^{-1}$)) in the positive and negative electrodes, respectively, and J is the current density (current per unit area ($A\,m^{-2}$)) transferred through the separator from the negative electrode to the positive electrode. Ω_p and Ω_n denote the domains of the positive and negative electrodes, respectively. According to Ohm's law, $\vec{i}_p$ and $\vec{i}_n$ can be written as follows:

$$\vec{i}_p = -\frac{1}{r_p}\nabla V_p \quad \text{in } \Omega_p \tag{3}$$

$$\vec{i}_n = -\frac{1}{r_n}\nabla V_n \quad \text{in } \Omega_n \tag{4}$$

where r_p and r_n are the resistances (Ω) of the positive and negative electrodes, respectively, and V_p and V_n are the potentials (V) of the positive and negative electrodes, respectively. The following Poisson equations for V_p and V_n were obtained by substituting Eqs. (3) and (4) into Eqs. (1) and (2):

$$\nabla^2 V_p = -r_p J \quad \text{in } \Omega_p \tag{5}$$

Table 1
Parameters used to calculate the electrode resistance.

Parameter	Li_xC_6	$Li[NiMnCo]O_2$
S_e ($S\,cm^{-1}$)	1.0	0.139
h_e (μm)	145	150
S_c ($S\,cm^{-1}$)	6.33×10^5	3.83×10^5
h_c (μm)	10	20

$$\nabla^2 V_n = +r_n J \quad \text{in } \Omega_n \tag{6}$$

The relevant boundary conditions for V_p and V_n are given in Ref. [17].

Regarding the electrode as the equivalent network of parallel-connected resistors of electrode material and current collector as in Ref. [28], the resistance, r (r_p or r_n), was calculated as follows:

$$r = \frac{1}{h_c S_c + h_e S_e} \tag{7}$$

where h_c and h_e are the thicknesses (m) of the current collector and the electrode material, respectively, and S_c and S_e are the electrical conductivities ($S\,m^{-1}$) of the current collector and the electrode material, respectively. The resistance calculated by Eq. (7) is dominated by the resistance of current collector and the potential distribution of the electrode is essentially governed by the potential distribution of the current collector. Table 1 lists the parameters used to calculate the resistances for the electrodes [17,25,26].

The current density, J, of Eqs. (5) and (6) is a function of the potential difference between the positive and negative electrodes ($V_p - V_n$). The functional form depends on the polarization characteristics of the electrodes. In this study, the following polarization expression used by Tiedemann and Newman [29] and Newman and Tiedemann [20] was adopted

$$J = Y(V_p - V_n - U) \tag{8}$$

where Y and U are the fitting parameters. As suggested by Gu [30], U and Y were expressed as functions of the depth of discharge (DOD) as follows:

$$U = a_0 + a_1(\text{DOD}) + a_2(\text{DOD})^2 + a_3(\text{DOD})^3 \tag{9}$$

$$Y = a_4 + a_5(\text{DOD}) + a_6(\text{DOD})^2 \tag{10}$$

where a_0–a_6 are constants to be determined experimentally. Fitting parameters used to calculate the potential and current-density distribution on the electrodes are listed in Table 2.

By solving the equations listed previously, the distribution of the current density, J, on the electrodes can be obtained as a function of the position on the electrode and time. Therefore, the DOD varies along with the position on the electrode and time elapsed during discharge. The distribution of DOD on the electrode can be calculated from the distribution of J as follows:

$$\text{DOD} = \frac{\int_0^t J\,dt}{Q_T} \tag{11}$$

Table 2
Fitting parameters used to calculate the potential and current-density distributions on the electrodes.

Parameter	Value
a_0 in Eq. (9) (V)	4.195
a_1 in Eq. (9) (V)	−3.678
a_2 in Eq. (9) (V)	18.922
a_3 in Eq. (9) (V)	−60.364
a_4 in Eq. (10) ($A\,m^{-2}$)	78.631
a_5 in Eq. (10) ($A\,m^{-2}$)	−543.405
a_6 in Eq. (10) ($A\,m^{-2}$)	4918.64

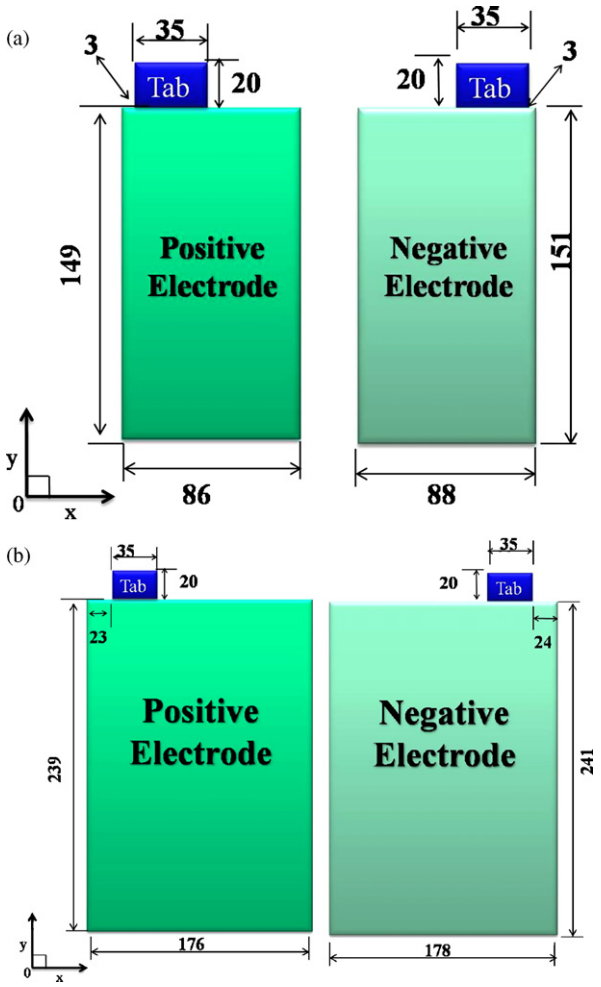

Fig. 2. Schematic diagram of the electrode shapes of the LIPB with the nominal capacities of (a) 10 Ah and (b) 26 Ah.

where t is the discharge time (s) and Q_T is the theoretical capacity per unit area (Ah m^{-2}) of the electrodes. The uniformity index, UI, of DOD is defined as

$$\mathrm{UI} = \frac{\mathrm{DOD_{max}} - \mathrm{DOD_{min}}}{2\mathrm{DOD}_{avg}} \tag{12}$$

where DOD_{max}, DOD_{min} and DOD_{avg} are the maximum, minimum and average values of the DOD on the electrodes, respectively. The uniformity of the DOD increases with decreasing UI. Therefore, a way of reducing UI should be devised in order to improve the uniform utilization of the active material of the electrodes and to lengthen the cycle life of the battery.

The thermal modeling procedure to calculate the temperature distribution on the electrodes is the same as that used by Kim et al. [27]. Since the thicknesses of the cell stacks are much shorter than the other dimensions of the electrodes shown in Fig. 2(a) and (b), the temperature variations across the cell stacks are neglected. Based on the differential energy conservation for a battery, the transient two-dimensional equation of heat conduction can be written as follows:

$$\rho C_p \frac{\partial T}{\partial t} = \frac{\partial}{\partial x}\left(k_x \frac{\partial T}{\partial x}\right) + \frac{\partial}{\partial x}\left(k_y \frac{\partial T}{\partial y}\right) + q - q_{conv} \tag{13}$$

where ρ is the density (kg m^{-3}), C_p is the volume averaged specific heat capacity at constant pressure (J kg^{-1} °C^{-1}), T is the temperature (°C), k_x and k_y is the effective thermal conductivity along the x and y directions (refer Fig. 1 for the x and y directions) (W m^{-1} °C^{-1}), respectively, q is the heat generation rate per unit volume (W m^{-3}), and q_{conv} is the heat dissipation rate (W m^{-3}) through the surfaces of the battery by convection. The effective thermal conductivities of various compartments of the cell can be estimated based on the equivalent networks of parallel and series thermal resistances of the cell components [11,16].

Table 3
Parameters used for the thermal modeling.

Component	Density (g cm^{-3})	Heat capacity (J g^{-1} K^{-1})	Thermal conductivity (W cm^{-1} K^{-1})
Current collector of positive electrode	2.7	0.9	2.38
Electrode material of positive electrode	1.5	0.7	0.05
Current collector of negative electrode	8.96	0.385	3.98
Electrode material of negative electrode	2.5	0.7	0.05
Separator	1.2	0.7	0.01
Pouch	1.15	1.9	0.16×10^{-2}

The heat generation rate, q, is given as follows:

$$q = aJ\left[E_{oc} - E - T\frac{dE_{oc}}{dT}\right] + a_p r_p i_p^2 + a_n r_n i_n^2 \tag{14}$$

where a is the specific area of the battery (m^{-1}), J is the current density (A m^{-2}) calculated by Eq. (8), E_{oc} is the open-circuit potential of the cell (V), E is the cell voltage (V), a_p and a_n are the specific area of the positive and negative electrodes (m^{-1}), respectively, and i_p and i_n are the magnitudes of the vectors $\vec{i}_p$ and $\vec{i}_n$ obtained by Eqs. (3) and (4) (A m^{-1}), respectively. The detailed definition of each term on the right-hand side of Eq. (14) is described in Refs. [27,31,32]. The heat dissipation rate, q_{conv}, is derived as follows

$$q_{conv} = \frac{2h}{d}(T - T_{air}) \tag{15}$$

where h is the convective heat transfer coefficient on the surfaces of the battery (W m^{-2} °C^{-1}), d is the thickness of the battery in the direction perpendicular to the parallel electrodes (m), and T_{air} is the ambient temperature (°C). This term is rendered by an approximation of a three-dimensional object into a two-dimensional one, as shown in Eq. (15). The convective boundary condition applied to the boundaries of the electrode is reported by Kim et al. [27]. Table 3 lists the parameters used for the thermal modeling.

3. Results and discussion

The solutions to the governing Eqs. (5), (6) and (13) subject to the associated boundary conditions were obtained using the finite element method. Although numerical simulations were performed for the electrodes of many different shapes of a LIPB, the results for the electrodes of Fig. 2 are shown because it is believed they are sufficient to demonstrate the salient features of the model presented in this paper. In order to test the validity of the model, discharge experiments were carried out at room temperature using a 10 Ah battery fabricated by VK Corporation, of which the dimensions of the electrodes and the positions of the tabs are shown in Figs. 2(a). 3(a) shows the calculated discharge curves from the model and experimental data. At various discharge rates from 0.5 to 5 C, the experimental discharge curves are in good agreement with the modeling results based on the finite element method. Fig. 3(b) shows the discharge curves predicted for a 26 Ah LIPB based on the same modeling parameters obtained for 10 Ah LIPB and the experimental data. Fig. 2(b) gives the dimensions of the electrodes and the positions of the tabs for the 26 Ah LIPB. At various discharge

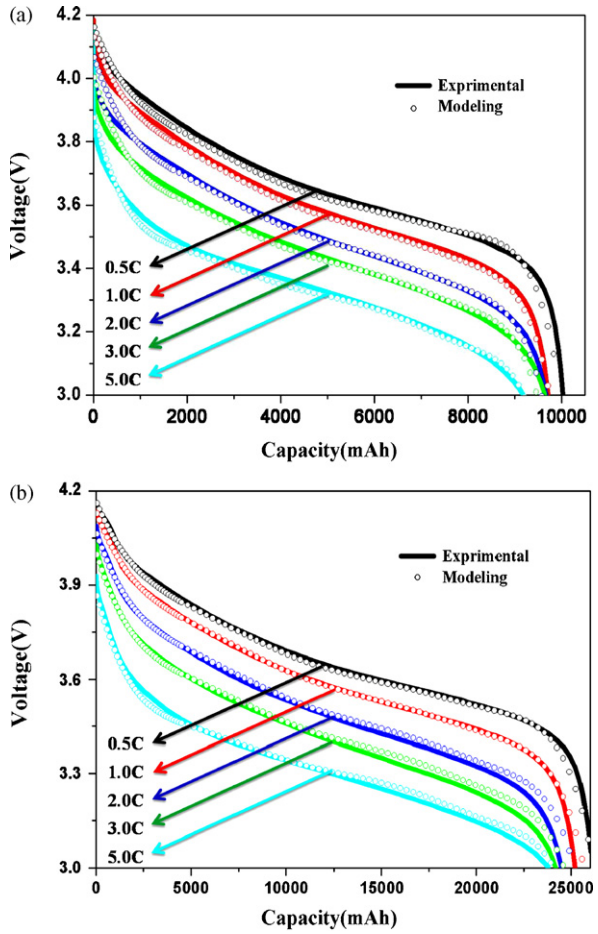

Fig. 3. Comparison of the experimental and modeling discharge curves at discharge rates ranging from 0.5 to 5 C for the LIPB with nominal capacities of (a) 10 Ah and (b) 26 Ah. The solid lines denote the experimental data and open circles are modeling results based on the finite element method.

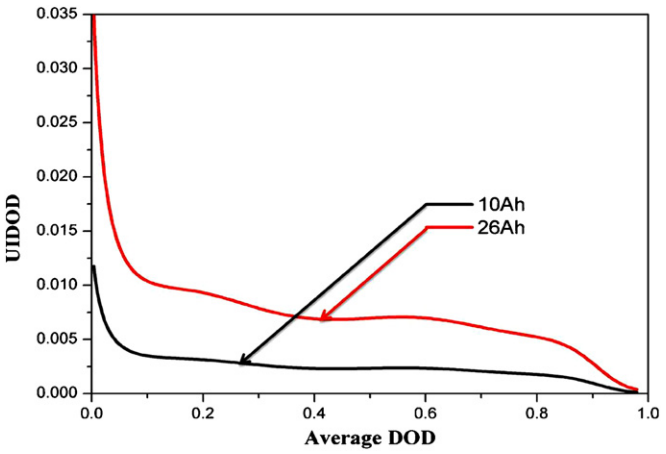

Fig. 4. Distribution of (a) the potential on the positive electrode, (b) the potential on the negative electrode, and (c) the current density on the electrodes for a 26 Ah LIPB at a discharge rate of 1 C for 30 min.

rates from 0.5 to 5 C, the experimental discharge curves are in good agreement with the modeling results. These results suggests that the modeling parameters obtained for a small-scale battery can be used to predict the discharge characteristics of a large-scale battery without additional adjustments of the parameters provided the materials and compositions of the electrodes as well as the fabrication parameters (in particular the loading or thickness of the porous electrode films) are the same. The model can be used to predict the effect of the configuration of the electrodes such as the aspect ratio of the electrodes and the size and placement of current collecting tabs on the uniformity of the utilization of the active material of electrodes as well as the discharge and thermal characteristics [17,27].

The distributions of the potential and current density on the electrodes during discharge were obtained as a function of time for various discharge rates. As an example, Fig. 4(a)–(c) shows the distributions of the potential on the positive electrode, the potential on the negative electrode, and the current density for the 26 Ah LIPB at a discharge time of 30 min at a rate of 1 C, respectively. In Fig. 4(a), the potential gradient on the positive electrode appears to be most severe in the region where the tab is attached to the current collector. This is because all the current flows through the conducting current collector into the tab from the entire electrode plate. Again, the potential gradient on the negative electrode shown in Fig. 4(b) is the highest at the region near the tab because all the current needs to flow from the tab through the entire electrode plate. Fig. 4(c) shows the non-uniform distributions of the current density transferred from the negative electrode to the positive electrode during discharge at a rate of 1 C. The distributions of the DOD on the electrodes can be obtained by integrating the current density with respect to time. The change in the UI of the DOD with time can be calculated based on the distributions of the DOD. Fig. 5 shows the UIs of the DOD of the 10 and 26 Ah LIPB as a function of the average DOD over the entire electrode area at a discharge rate of 1 C. The UI of the DOD maintains a higher value for the 26 Ah LIPB than for the 10 Ah LIPB throughout the whole stages of discharge. This trend shows that the non-uniformity of the utilization of the active material of the electrodes becomes more pronounced as the size of the electrode increases, because the uniformity of the DOD increases with decreasing UI based on the definition of UI. Once the capacity of the LIPB is given, such calculations for the electrodes of different shapes can be iterated limitlessly in order to optimize the design of the electrode configuration, as discussed by Kwon et al. [17].

After obtaining the distributions of the potential and current density on the electrodes during discharge, the temperature distributions of the battery can be calculated as a function of time at various discharge rates using Eq. (13). As a demonstration, Fig. 6 shows the temperature distributions based on the experimental IR image and the modeling for the 26 Ah LIPB after the discharge for 10.8 min at a rate of 5 C. The overall temperature distributions from the experiment and model are in good agreement. The temperature near the current collecting tab of the positive electrode is higher than that of the negative electrode. This was attributed to the electrical conductivity of the active material of the positive electrode being much lower than that of the negative electrode, even though both the current flows near the tabs of the positive and negative electrodes are similarly high. The maximum temperatures from the experiment and model were similar, approximately 63 °C, even though the minimum temperature from the experiment is slightly higher than that from the model. Fig. 7(a) and (b) shows the maximum and minimum temperatures from the experimental measurements for the 26 Ah LIPB and those predicted by the model, respectively. The maximum temperatures from the experiment and modeling were in good agreement over the whole range of DODs at various discharge rates. However, the discrepancy between the minimum temperatures from the experiment and modeling increased for DOD values >0.5 at discharge rates of 1 and 3 C. As we may notice from Fig. 6(a) and (b), the temperatures of the corners of the electrodes have the minimum values, where the

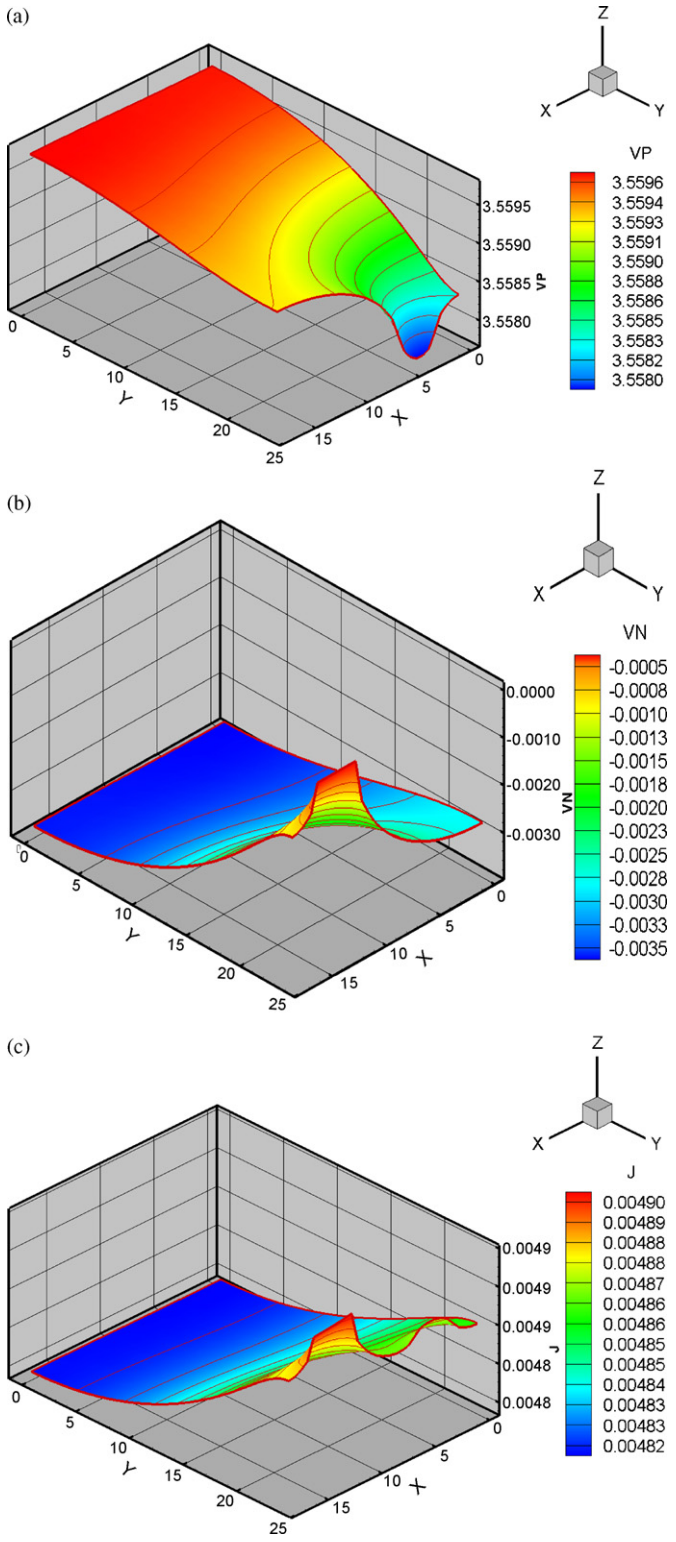

Fig. 5. UIs of the DOD for the LIPB with nominal capacities of 10 and 26 Ah as a function of the average DOD at a discharge rate of 1 C.

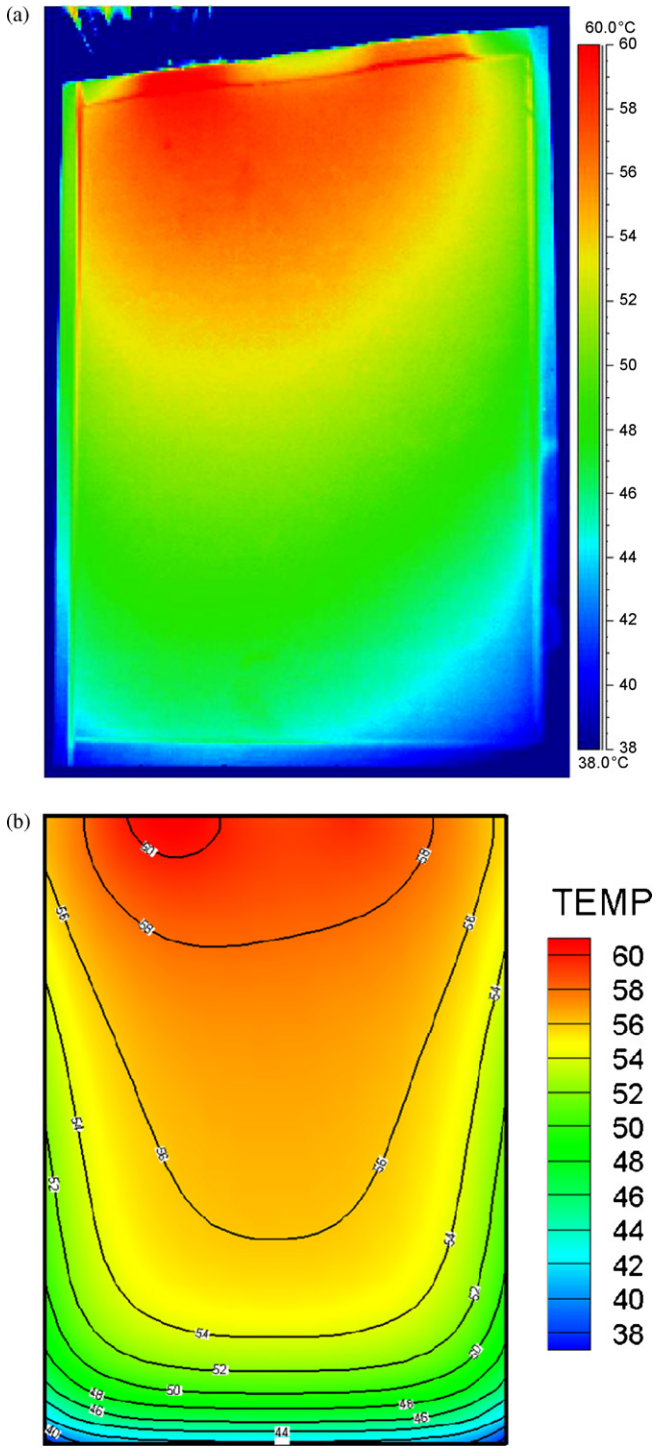

Fig. 6. Temperature distributions based on (a) the experimental IR image and (b) the modeling for the LIPB of 26 Ah at a discharge rate of 5 C for 10.8 min.

effect of two-dimensional approximation of the three-dimensional LIPB on the accuracy of the thermal modeling is maximal. Therefore, the two-dimensional model of this work was unable to pick up the physics of the system accurately for the minimum temperatures. The model may improve for the minimum temperatures, if it is extended to three-dimensional, which is beyond the scope of this work. In Fig. 8, the maximum temperatures from the experimental measurements for the 26 and 10 Ah LIPBs were compared with those predicted by the model. Although the difference between the maximum temperatures of the 26 and 10 Ah LIPBs were minute at a discharge rate of 1 C, at a discharge rate of 5 C, the maximum temperature of the 26 Ah LIPB was higher than that of the 10 Ah LIPB. This suggests that the optimal design of the larger electrode of the LIPB is essential for preventing possible significant temperature increases during high power extraction.

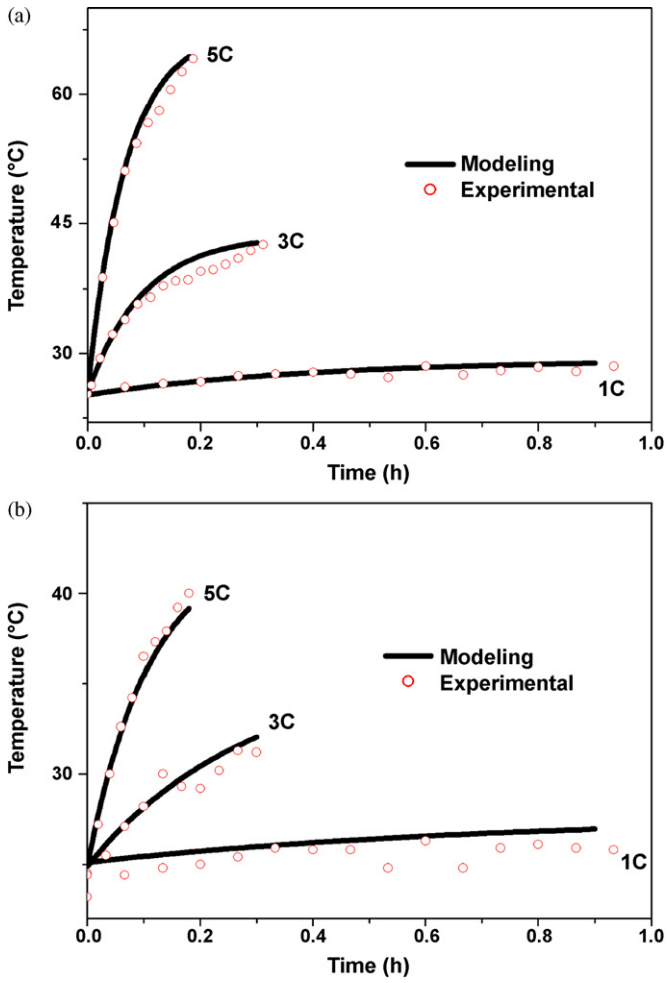

Fig. 7. Comparison of (a) the maximum temperatures and (b) the minimum temperatures from the experiment and model for a 26 Ah LIPB at discharge rates of 1, 3, and 5 C.

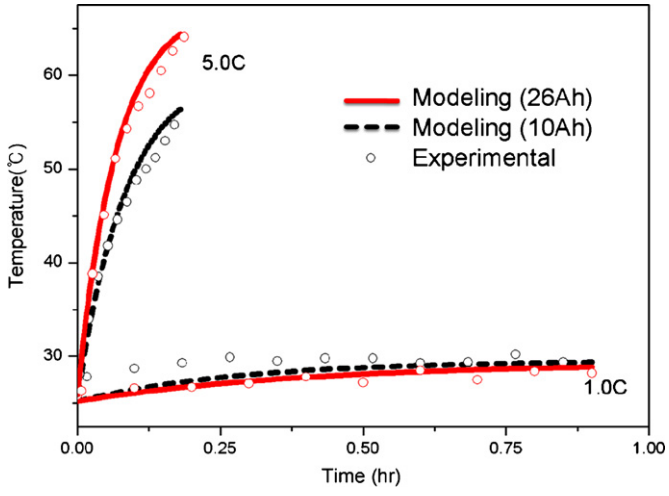

Fig. 8. Comparison of the maximum temperatures from the experiment and model for 10 and 26 Ah LIPBs at discharge rates of 1 and 5 C.

4. Conclusions

A mathematical procedure was developed for the scale-up of a LIPB. The two-dimensional potential and current-density distribution on the electrodes of a LIPB were predicted as a function of the discharge time using the finite element method. By comparing the experimental discharge curves of 10 and 26 Ah LIPBs with the modeling results at discharge rates ranging from 0.5 to 5 C, it was confirmed that the parameters tuned for the electrodes of a small-scale battery can be applied for the electrodes of a large-scale battery provided the materials and compositions of the electrodes as well as the manufacturing processes are the same. Based on the modeling results of the potential and current-density distributions, the heat generation rate as a function of the discharge time and position on the electrodes was calculated to predict the thermal behavior of the LIPB. The two-dimensional temperature distributions from the experiment and model were in good agreement. The modeling methodology presented in this study, which adopted a relatively simpler modeling approach than in previous studies, may contribute to the scale-up of the LIPB and modification of the electrode configuration.

Acknowledgements

This study was supported by the Ministry of Commerce, Industry, and Energy of Republic of Korea under the Generic Technology Development Program. One of the authors (C.B. Shin) acknowledges the Korea Science and Engineering Foundation (KOSEF R01-2006-000-10239-0) and the Ministry of Commence, Industry and Energy of Republic of Korea (2007-E-1D25-P-02-0-00) for providing partial financial support for this work.

References

[1] G. Cedar, M. Doyle, P. Arora, Y. Fuentes, MRS Bull. 27 (2002) 619–623.
[2] M. Doyle, T.F. Fuller, J. Newman, J. Electrochem. Soc. 140 (1993) 1526–1533.
[3] P. Arora, R.E. White, M. Doyle, J. Electrochem. Soc. 145 (1998) 3647–3667.
[4] G.G. Botte, V.R. Subramanian, R.E. White, Electrochim. Acta 45 (2000) 2595–2609.
[5] J. Newman, K.E. Thomas, H. Hafezi, D.R. Wheeler, J. Power Sources 119–121 (1990) 838–843.
[6] C.R. Pals, J. Newman, J. Electrochem. Soc. 142 (1995) 3274–3281.
[7] C.R. Pals, J. Newman, J. Electrochem. Soc. 142 (1995) 3282–3288.
[8] S. Al-Hallaj, J.R. Selman, J. Power Sources 110 (2002) 341–348.
[9] K. Smith, C.-Y. Wang, J. Power Sources 160 (2006) 662–673.
[10] Y. Chen, J.W. Evans, J. Electrochem. Soc. 140 (1993) 1833–1838.
[11] Y. Chen, J.W. Evans, J. Electrochem. Soc. 141 (1994) 2947–2955.
[12] Y. Chen, J.W. Evans, J. Electrochem. Soc. 143 (1996) 2708–2712.
[13] L. Song, J.W. Evans, J. Electrochem. Soc. 145 (1998) 2327–2334.
[14] L. Song, J.W. Evans, J. Electrochem. Soc. 147 (2000) 2086–2095.
[15] P.M. Gomadam, J.W. Weidner, R.A. Dougal, R.E. White, J. Power Sources 110 (2002) 267–284.
[16] S.C. Chen, C.C. Wan, Y.Y. Wang, J. Power Sources 140 (2005) 111–124.
[17] K.H. Kwon, C.B. Shin, T.H. Kang, C.-S. Kim, J. Power Sources 163 (2006) 151–157.
[18] M.W. Verbrugge, J. Electrostatics 34 (1995) 61–85.
[19] D.R. Baker, M.W. Verbrugge, J. Electrochem. Soc. 146 (1999) 2413–2424.
[20] J. Newman, W. Tiedemann, J. Electrochem. Soc. 140 (1993) 1961–1968.
[21] G. Sikha, B.N. Popov, R.E. White, J. Electrochem. Soc. 151 (2004) A1104–A1114.
[22] G. Ning, B.N. Popov, J. Electrochem. Soc. 151 (2004) A1584–A1591.
[23] G. Ning, R.E. White, B.N. Popov, Electrochim. Acta 51 (2006) 2012–2022.
[24] D.W. Dees, V.S. Battaglia, A. Bélanger, J. Power Sources 110 (2002) 310–320.
[25] M. Doyle, J. Newman, A.S. Gozdz, C.N. Schmutz, J.-M. Tarascon, J. Electrochem. Soc. 143 (1996) 1890–1903.
[26] P. Arora, M. Doyle, A.S. Gozdz, R.E. White, J. Newman, J. Power Sources 88 (2000) 219–231.
[27] U.S. Kim, C.B. Shin, C.-S. Kim, J. Power Sources 180 (2008) 909–916.
[28] Y. Morimoto, Y. Ohya, K. Abe, T. Yoshida, H. Morimoto, J. Electrochem. Soc. 135 (1988) 293–298.
[29] W. Tiedemann, J. Newman, in: S. Gross (Ed.), The Electrochemical Society, Princeton, NJ, 1979, pp. 39–49.
[30] H. Gu, J. Electrochem. Soc. 130 (1983) 1459–1464.
[31] C.Y. Wang, V. Srinivasan, J. Power Sources 110 (2000) 364–376.
[32] V. Srinivasan, C.Y. Wang, J. Electrochem. Soc. 150 (2003) A98–A106.